

Structure-Based Discovery of Novel Nonpeptide Inhibitors Targeting SARS-CoV-2 M^{pro}

Jingyi Yang, Xiaoyuan Lin, Na Xing, Zhao Zhang, Haiwei Zhang, Haibo Wu,* and Weiwei Xue*



Cite This: <https://doi.org/10.1021/acs.jcim.1c00355>



Read Online

ACCESS |



Metrics & More

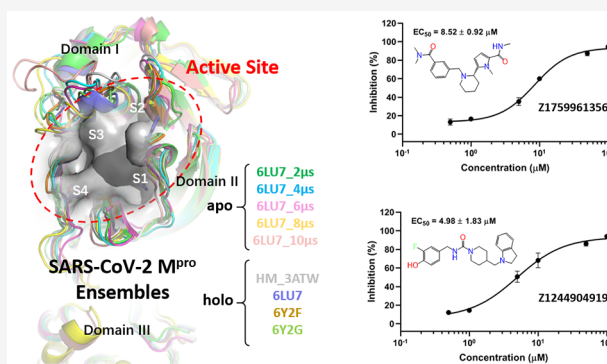


Article Recommendations



Supporting Information

ABSTRACT: The continual spread of novel coronavirus disease 2019 (COVID-19) is caused by severe acute respiratory syndrome coronavirus 2 (SARS-CoV-2), posing a severe threat to the health worldwide. The main protease (M^{pro}, alias 3CL^{pro}) of SARS-CoV-2 is a crucial enzyme for the maturation of viral particles and is a very attractive target for designing drugs to treat COVID-19. Here, we propose a multiple conformation-based virtual screening strategy to discover inhibitors that can target SARS-CoV-2 M^{pro}. Based on this strategy, nine M^{pro} structures and a protein mimetics library with 8960 commercially available compounds were prepared to carry out ensemble docking for the first time. Five of the nine structures are apo forms presented in different conformations, whereas the other four structures are holo forms complexed with different ligands. The surface plasmon resonance assay revealed that 6 out of 49 compounds had the ability to bind to SARS-CoV-2 M^{pro}. The fluorescence resonance energy transfer experiment showed that the biochemical half-maximal inhibitory concentration (IC₅₀) values of the six compounds could hamper M^{pro} activities ranged from 0.69 ± 0.05 to 2.05 ± 0.92 μM. Evaluation of antiviral activity using the cell-based assay indicated that two compounds (Z1244904919 and Z1759961356) could strongly inhibit the cytopathic effect and reduce replication of the living virus in Vero E6 cells with the half-maximal effective concentrations (EC₅₀) of 4.98 ± 1.83 and 8.52 ± 0.92 μM, respectively. The mechanism of the action for the two inhibitors were further elucidated at the molecular level by molecular dynamics simulation and subsequent binding free energy analysis. As a result, the discovered noncovalent reversible inhibitors with novel scaffolds are promising antiviral drug candidates, which may be used to develop the treatment of COVID-19.



INTRODUCTION

Infection with severe acute respiratory syndrome coronavirus 2 (SARS-CoV-2) will cause novel coronavirus disease 2019 (COVID-19),¹ and the pandemic of the disease has rapidly become a global health concern² and led to 160,074,167 confirmed cases and 3,325,260 deaths worldwide as of May 13, 2021.¹ To cope with the severe crisis, great efforts have been paid to developing therapeutic approaches and vaccines against SARS-CoV-2.^{3,4} Discovering inhibitors of key proteins involved in the viral life cycle is an often-used and efficient approach to disrupt the replication of virus.⁵ Like SARS-CoV, the encoded 4 structural and 16 nonstructural proteins (NSPs) of SARS-CoV-2 provide multiple avenues to identify potential drug targets.^{6,7} Among the encoded proteins, the main protease (M^{pro}, alias 3CL^{pro}), which has no human homolog, has become an attractive therapeutic target for the drug discovery and development of anti-COVID-19.^{8,9}

M^{pro} belongs to the 16 NSPs of coronavirus (CoV) and is a vital enzyme that has an essential role in mediating the replication and transcription of CoVs.⁸ Together with papain-like proteases (PLPs), the enzyme processes the polyproteins that are translated from CoV RNA.¹⁰ M^{pro} is a highly conservative protein existing in all CoVs consisting of three

domains (domains I to III).⁸ Crystal structures of SARS-CoV-2 M^{pro} (Figure 1)^{9,11} show that they are the chymotrypsin-like domain (domain I, residues 10 to 99), picornavirus 3C protease-like domain (domain II, residues 100 to 182), and a globular cluster formed by five helices (domain III, residues 198 to 303). The substrate-binding site (active site) of M^{pro} composed of four subsites (S1, S2, S3, and S4) is located at the six-stranded antiparallel β barrels between domains I and II.⁹

Based on the crystal structures of SARS-CoV or SARS-CoV-2 M^{pro}, computer-aided drug design techniques have been successfully used in anti-COVID-19 studies regarding the rapid discovery of potential inhibitors,^{12–16} drug repurposing,^{14,16–20} and making the action mechanism of the active compound against SARS-CoV-2 more understandable.²¹ Though these timely research studies have led to the design of several first-in-

Received: March 26, 2021

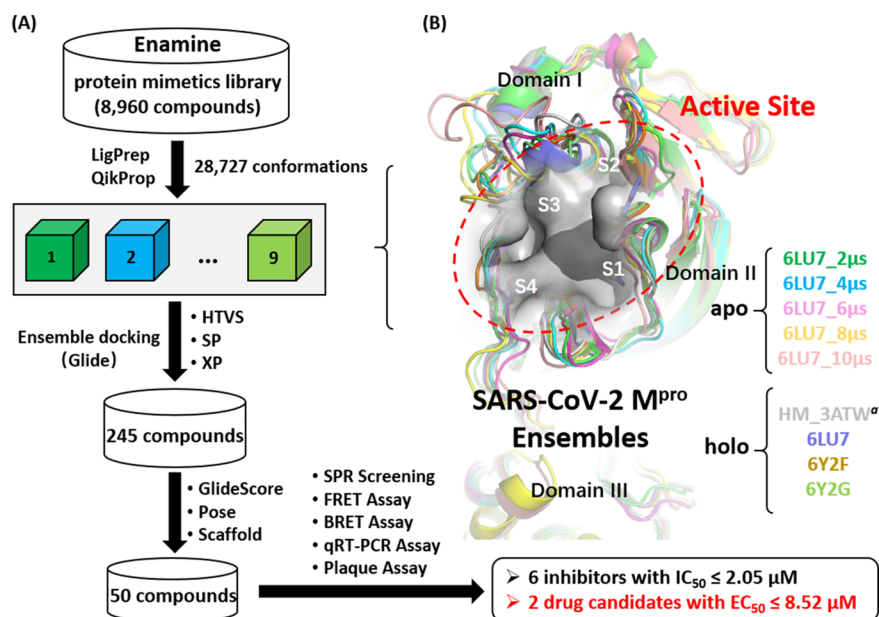


Figure 1. (A) Workflow of ensemble docking-based virtual screening of novel nonpeptide inhibitors targeting SARS-CoV-2 M^{pro}. (B) Ensemble SARS-CoV-2 M^{pro} 3D structures shown in cartoon representation with different colors. Domain I (residues 10 to 99), Domain II (residues 100 to 182), and Domain III (residues 198 to 303) of the protease are labeled. The substrate-binding site (active site) of M^{pro} composed of four subsites (S1', S1, S2, and S4) marked by the gray surface.

class SARS-CoV-2 M^{pro} inhibitors as promising drug candidates,^{8,9,11} currently no M^{pro}-based therapeutics have been officially approved for COVID-19.³ The need to develop novel as well as more effective antiviral drugs to inhibit SARS-CoV-2 has become more urgent.³ However, larger flexibility and figurability of active sites on SARS-CoV-2 M^{pro} proved to be a challenge for the rational design of small molecule inhibitors.^{22,23} For addressing this problem, the crystal structures of M^{pro} could be complemented by the all-atom molecular dynamics (MD) trajectory data released publicly in the spirit of open science.^{24,25}

In the present work, based on nine different conformations of the SARS-CoV-2 M^{pro} substrate-binding site, a multiple conformational-based virtual screening strategy in combination with experimental validation was proposed to identify the enzyme inhibitors from a protein mimetics library with 8960 commercially available compounds (Figure 1). Considering the docking pose and scaffold diversity, 49 selected candidates were purchased for testing their binding profiles to SARS-CoV-2 M^{pro} using the surface plasmon resonance (SPR) assay. The identified six compounds were further evaluated by the fluorescence resonance energy transfer assay (enzyme kinetics study) and bioluminescence resonance energy transfer (BRET) assay. All six compounds showed inhibition activities against the cell lines of SARS-CoV-2 M^{pro}. The live virus assay indicated that two out of the six inhibitors had the activity to interdict the viral infection of SARS-CoV-2. In addition, computational absorption-distribution-metabolism-excretion (ADME) analysis showed that the two inhibitors had good pharmacokinetic properties and low toxicity.

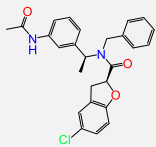
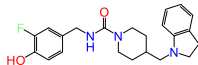
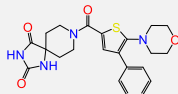
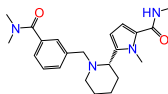
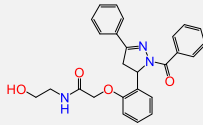
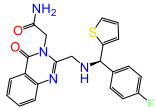
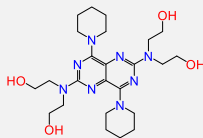
RESULTS AND DISCUSSION

Compounds Selected through Ensemble Docking. To account for protein flexibility, nine M^{pro} ensembles including five MD-sampled apo structures and four holo structures (one homology model and three crystal structures in complex with

different ligands) were collected. Meanwhile, a protein mimetics library (with 8960 compounds) from Enamine was prepared and resulted in 28,727 conformations. As an initial step, ensemble docking of the prepared library against the active site of the defined nine M^{pro} ensembles was performed to identify potential lead candidates. By considering the GlideScore, binding pose, and scaffold diversity profiles, the nine sets of hits from the ensemble docking were then used for selecting 50 top-ranked compounds (with 49 purchased) for experimental testing using SPR assays. As shown in Table S1, the selected compounds as potential M^{pro} inhibitors have GlideScore ≤ -5.651 kcal/mol, and each of the compound forms at least two hydrogen bonds with the residues located at the protease active site. The hierarchical clustering of the fingerprints using Tanimoto similarity and Ward's cluster linkage method²⁶ of the selected compounds shown in Figure S1 indicated the high diversity of the scaffolds. HPLC chromatograms and mass spectrograms were applied to verify the chemical structures and purity of the 49 compounds, and the data of the six active compounds (see the next section) are provided in the Supporting Information.

Evaluation of Compounds as Inhibitors of SARS-CoV-2 M^{pro} In Vitro. By using dipyrindamole (DIP) as a positive control, the binding toward SARS-CoV-2 M^{pro} of the purchased 49 compounds was tested using the SPR assay at 100 μM concentrations (Figure S2). In addition, 6 out of the 49 compounds that have the abilities of binding to M^{pro} (Table 1) were selected to investigate whether their binding alters the biochemical function of the enzyme. The ranking of GlideScore for the six compounds Z236230776, Z1244904919, Z225729516, Z1759961356, Z108564100, and Z106460362 was 42/50, 33/50, 19/50, 25/50, 11/50, and 1/50, respectively. There is only one compound (Z106460362) that was at the top 10 of the list (Table S1). Furthermore, we determined the biochemical half-maximal inhibitory concentration (IC_{50}) values of the six chemical compounds, ranging from 0.69 to 2.05 μM (Figure 2). All compounds presented a

Table 1. Information of Six Compounds That Have the Abilities of Binding to M^{Pro} Using Dipyridamole (DIP) as a Positive Control

No.	IDs	RU ^a	M ^{Pro} ensembles ^b	GlideScore ^c	Chemical structures
1	Z236230776	25.2	6LU7_4us	-7.343	
2	Z1244904919	21.1	HM_3ATW	-7.651	
3	Z225729516	21.1	6Y2F	-8.502	
4	Z1759961356	19.2	6Y2F	-8.332	
5	Z108564100	17.1	6Y2F	-8.718	
6	Z106460362	15.6	6Y2G	-9.415	
DIP	-	21	-	-	

^aThe resonance units (RU) of the SPR assay in the presence of each compound at a concentration of 100 μM . ^bThe nine SARS-CoV-2 M^{Pro} structures including five apo forms (extracted per 2 μs from 10 μs MD simulation of 6LU7¹¹) and the four holo forms (one homology model using 3ATW³³ as a template and three crystal structures 6LU7,¹¹ 6Y2F,⁹ and 6Y2G⁹ in complex with different ligands). ^cThe docking scores (kcal/mol) were calculated by the Glide extra precision algorithm.³⁹

strong inhibitory effect on M^{Pro} activity, among which Z1759961356 ($\text{IC}_{50} = 0.69 \pm 0.05 \mu\text{M}$) had the strongest effect (Figure 2). Consistent with the IC_{50} results, the BRET ratio showed that all compounds had a good inhibitory effect on M^{Pro} in HEK293T cells (Figure 3). However, in this structure-based virtual screening study, although multiple conformation strategy was employed, the success rate was still very low (only 12% cases were correctly predicted by Glide docking). It is hypothesized that this is because those compounds were selected from specific conformations of the SARS-CoV-2 M^{Pro}. However, according to the experimental test, the specific structure may not occupy the preferred conformation of the protease. Therefore, to increase the success rate of virtual screening, enhanced conformational sampling of the protease by state-of-the-art MD simulation is needed. In addition, the flexibility of the protease active site was not considered during each docking process, which was crucial for the protein–ligand recognition. Therefore, the induced fit docking method may be used to address this problem even if the calculation is time consuming.

Inhibitors Suppress SARS-CoV-2 Infection In Vitro.

For examining whether these two lead candidates could prevent viral replication, further qRT-PCR and plaque-

reduction assays were carried out in Vero E6 cells infected by SARS-CoV-2. As can be seen from Figure 4, quantitative qRT-PCR results showed that Z1244904919 and Z1759961356 exhibited a stronger effect on anti-SARS-CoV-2 (Figure 4A,B). The plaque-reduction assay indicated that Z1244904919 and Z1759961356 displayed inhibitory effect on SARS-CoV-2, and the individual EC_{50} values were $4.98 \pm$ and $8.52 \pm \mu\text{M}$, respectively (Figure 4C,D). Furthermore, the SPR assay showed that Z1244904919 and Z1759961356 bound to SARS-CoV-2 M^{Pro} with K_d values of 465 and 133 μM , respectively (Figure 5A,B). In conclusion, these data suggest that the inhibition of Z1244904919 and Z1759961356 on M^{Pro} is mainly achieved through direct binding to the enzyme active site.

MD Simulation of the Inhibitor–M^{Pro} Complex.

Though the two lead candidates were recognized by ensemble docking, we thought that their predicted binding modes in M^{Pro} were not enough because the protease flexibility was not considered in each independent docking. To investigate inhibitor–M^{Pro} interaction flexibility, 1 μs MD simulation was executed for sampling enough conformations of the two complexes. The root-mean-square deviation (RMSD) of the backbone atoms on protein and heavy atoms on the ligand

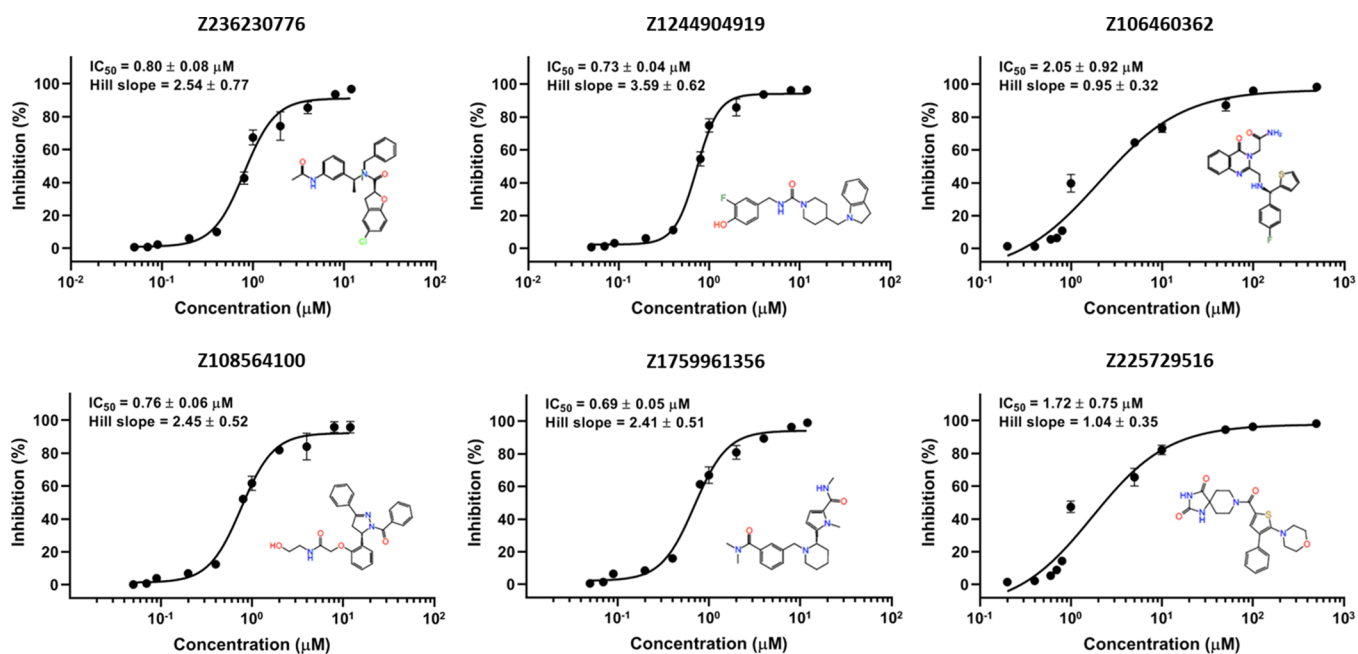


Figure 2. Inhibitory activity profiles of compounds against SARS-CoV-2 M^{Pro} . The median inhibitory concentration (IC_{50}) values were determined by a fluorescence resonance energy transfer (FRET)-based cleavage assay.

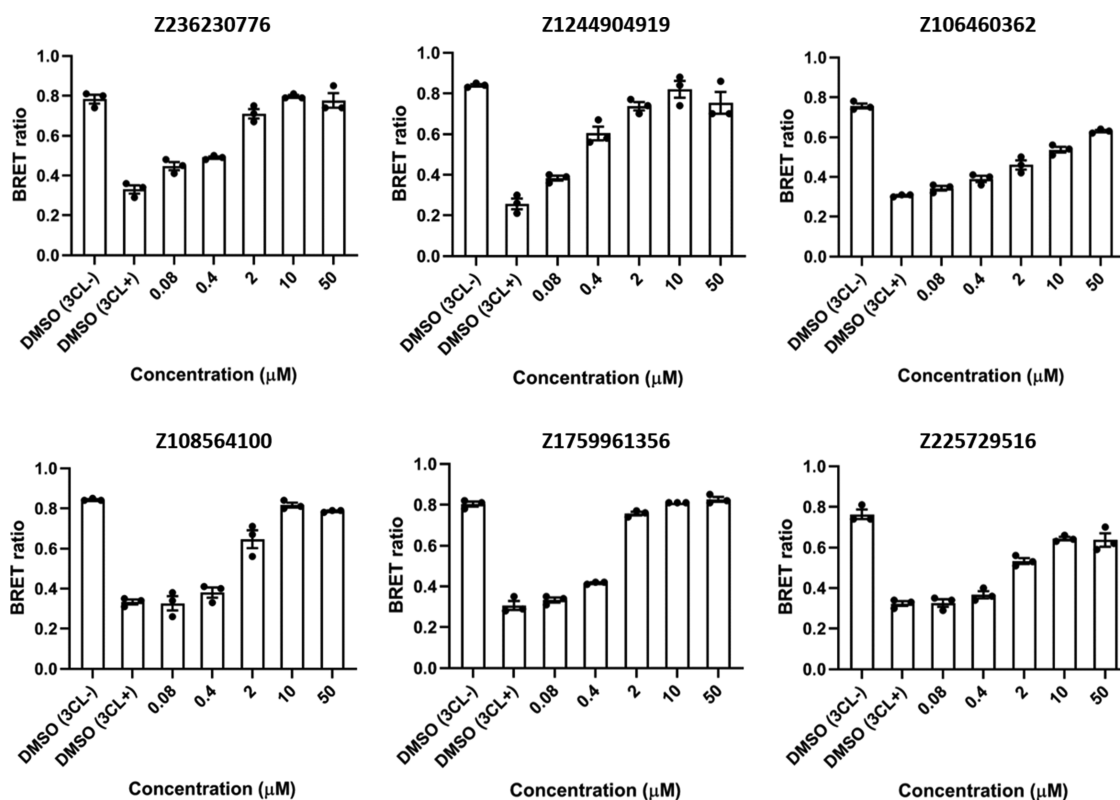


Figure 3. Dose dependence of six inhibitors on intracellular SARS-CoV-2 M^{Pro} activity measured using a bioluminescence resonance energy transfer (BRET) ratio.

referred to the starting structure was computed to reflect the stabilities of the studied systems during the period of simulation (Figure S3). The RMSD value variation suggested that the two complexes had small changes of conformation on the process of simulation. The average RMSD values of the binding site residues for Z1244904919 and Z1759961356 bound M^{Pro} were 0.88 and 1.86 Å, respectively. The values for

Z1244904919 and Z1759961356 were 1.09 and 1.96 Å. The trends of RMSD variation in Figure S3 indicated that the poses of ligands predicted were consistent with the active site of M^{Pro} . In addition, we have compared the predicted poses of inhibitors Z1244904919 and Z1759961356 with positive control DIP in M^{Pro} (Figure S4A,B). The results showed that

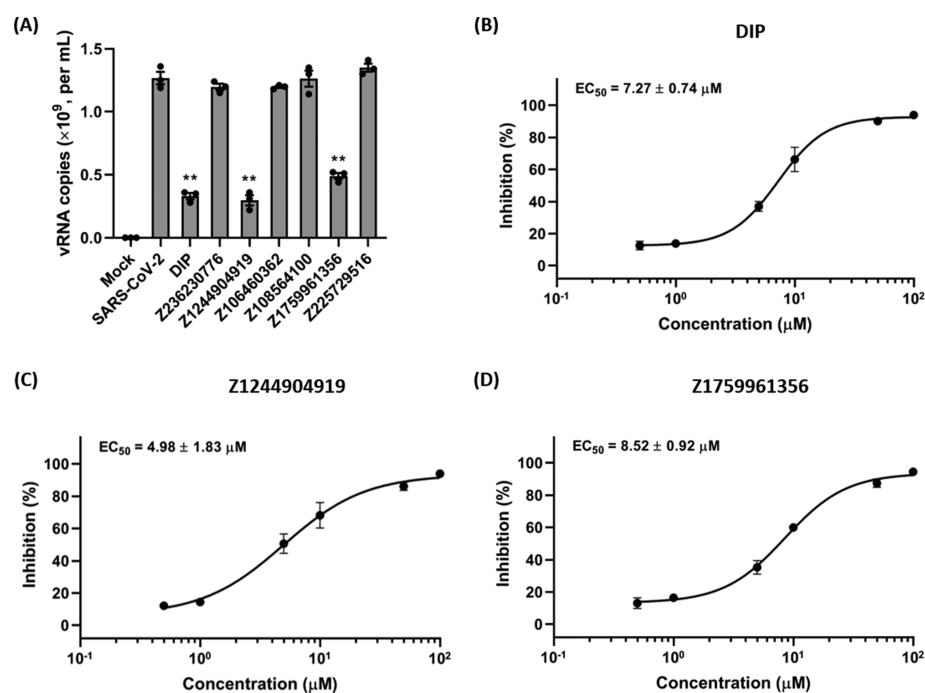


Figure 4. In vitro inhibition of viral main protease inhibitors against SARS-CoV-2. (A) At 72 h after infection, viral RNA (vRNA) copy numbers in Vero E6 cells monitored by qRT-PCR. (B–D) Mean percent inhibition of virus yield in the cells treated with a series concentration of DIP, Z1244904919, and Z1759961356.

the three ligands occupied the same binding site of the protease.

Binding Free Energy and Interaction Mode of Inhibitors in M^{Pro} . On the account of the MD trajectories, the binding free energy of the two inhibitors bound to M^{Pro} (ΔG_{calc}) was estimated using the MM/GBSA method.²⁷ As shown in Table 2, the ΔG_{calc} for Z1244904919 and Z1759961356 bound to M^{Pro} was -45.72 and -48.01 kcal/mol, respectively. The variation trend of ΔG_{calc} values is compatible with the order of the experimental binding free energies (ΔG_{exp}). The energy terms of ΔG_{calc} are listed in Table 2, indicating that the electrostatic (ΔE_{ele}) and hydrophobic ($\Delta E_{\text{vdw}} + \Delta G_{\text{nonpol}}$) interactions were of great importance for the binding of the four anticoagulants; however, polar solvent energies (ΔG_{polar}) were not conducive to the binding of inhibitors. In order to acquire a more particular understanding of the protein–ligand interaction, we decomposed the binding free energies into each residue. Residues with an absolute energy contribution of ≥ 0.5 kcal/mol would be identified as key residues, which were conducive to the binding of inhibitors to the pocket; these key residues are displayed in Table S2. Meanwhile, the recognized key residues of the two complexes suggested that there was a certain degree of similar interactions between them. As shown in Table S2, a total of 14 and 13 residues in SARS-CoV-2 M^{Pro} were identified to play an important role in Z1244904919 and Z1759961356 binding, respectively. Compared with the characterized interactions between the protease with the substrate²⁸ and N3,²⁹ 10, 6, 7, and 5 common residues were found for Z1244904919- and Z1759961356-bound complexes (Figure S5), indicating that the key interactions between the protease pocket and ligands were maintained for the identified new nonpeptide inhibitors. Meanwhile, the superposition between SARS-CoV-2 M^{Pro} in complex with N3 and Z1244904919 (Figure S4C) and ZN1759961356 (Figure

4D) indicates the overlap between the occupied pockets of these inhibitors, especially N3 and ZN1759961356.

The binding modes of Z1244904919 (Figure 5C) and Z1759961356 (Figure 5D) were investigated by the representative conformations extracted from the MD trajectories. As is known, the active site of M^{Pro} consists of four subpockets, which are S1, S2, S3, and S4.⁹ Residues Leu27, His41, Met49, His164, Met165, and Gln189 identified as key residues were of great importance for both Z1244904919- M^{Pro} (Figure 5E) and Z1759961356- M^{Pro} (Figure 5F) complexes. All the identified key residues uniformly distributed in the four subpockets of the M^{Pro} active site (Figure 5C,D). Taking Z1244904919 as an example (Figure 5C), the backbone atoms of Gly143, Ser144, Cys145, and Asn166 interact with the compound via hydrogen bonds. The fluorophenol moiety of Z1244904919 embedded into the S1 site consisted of residues Phe140 and Asn166, and the piperidine moiety took up the S4 site containing residues M165 and Gln189, while the indole analogue moiety and linkages in contact with residues Met49, Thr25, and His41 located at the S2 and S3 sites. The piperidine moiety acts like a linker to connect fluorophenol and indole analogue motifs. Compared to Z1244904919, the higher binding abilities of the Z1759961356 may come from the energy contributions of residues His164 and Met165 in the S1 pocket and residue Asn47 in the S2 pocket of the M^{Pro} active site. In this study, histidine (His41, His163, and His164) and cysteine (Cys145) located at the binding site of inhibitors were treated as neutral states during docking and MD simulation. However, it is important to note that the altering protonation states of titratable groups in histidine and cysteine in SARS-CoV-2 M^{Pro} , which can modulate protein dynamics and stability, is important in virtual screening studies. This has been well studied in the recently published work by Pavlova et al.³⁰

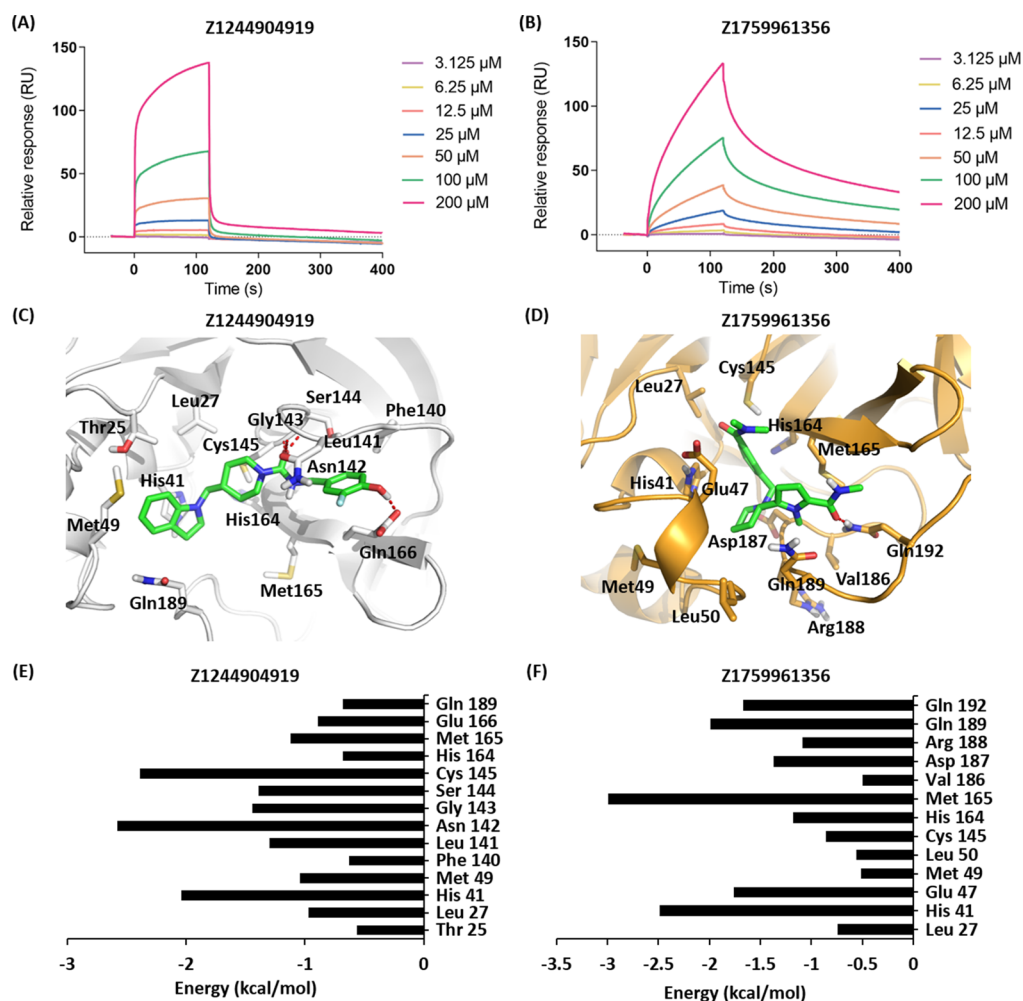


Figure 5. Binding of inhibitors to SARS-CoV-2 M^{Pro}. (A, B) Surface plasmon resonance (SPR) assay of Z1244904919 and Z1759961356 bound to the protease. (C, D) The binding modes and (E, F) energy contributions of key residues in the M^{Pro} active site for Z1244904919 and Z1759961356 to the protease. The protein and ligand were displayed as cartoon and stick representation, respectively. The hydrogen bond is shown in green dashed lines.

Table 2. Biochemical Half-Maximal Inhibitory Concentration (IC₅₀, μM) and Binding Free Energies (ΔG, kcal/mol) of Z1244904919 and Z1759961356 to M^{Pro}

complexes	ΔE _{ele} ^a	ΔE _{vdW} ^b	ΔG _{pol} ^c	ΔG _{nonpol} ^d	ΔG _{calc} ^e	IC ₅₀	ΔG _{exp} ^f
Z1244904919-M ^{Pro}	-18.76	-46.88	-65.63	-3.81	-45.72	0.73 ± 0.05	-8.70
Z1759961356-M ^{Pro}	-6.03	-52.51	-58.54	-4.25	-48.01	0.69 ± 0.05	-8.73

^aElectrostatic (ΔE_{ele}) energy terms in the gas phase. ^bvan der Waals (ΔE_{vdW}) energy terms in the gas phase. ^cPolar (ΔE_{pol}) solvent energies by solving the GB equation. ^dNonpolar (ΔE_{nonpol}) solvent energies by solving the GB equation. ^eCalculated binding free energy (ΔG_{calc}), ΔG_{calc} = ΔE_{ele} + ΔE_{vdW} + ΔE_{pol} + ΔE_{nonpol}. ^fExperimental binding free energy (ΔG_{exp}), ΔG_{exp} ≈ RTln(IC₅₀).

Table 3. Calculated Pharmacokinetic Properties of Compounds from QikProp (Version 4.5)

compounds	MW ^a	QPlogP _{o/w} ^b	QPlogS ^c	QPP _{Caco} ^d	absorption ^e
Z1244904919	383.465	3.408	-3.241	255.308	89.98
Z1759961356	382.505	2.899	-2.93	550.893	92.983
13a ^f	585.699	2.782	-5.863	29.197	43.542
13b ^f	593.678	2.682	-3.504	67.514	49.474
DIP ^g	504.631	1.974	-3.468	120.031	49.804

^aThe molecular weight of the molecule. ^bThe predicted log of the octanol/water partition coefficient. ^cThe predicted aqueous solubility; S in mol/L. ^dPredicted Caco-2 cell permeability in nm/s. ^ePredicted percent of human oral absorption (%). ^f13a and 13b are two recently reported two SARS-CoV-2 M^{Pro} inhibitors with favorable pharmacokinetic properties. ^gDIP is an FDA approved drug³² S4. The range or recommend values of MW (130.0 to 725.0), QPlogP_{o/w} (-2.0 to 6.5), QPlogS (-6.5 to 0.5), QPP_{Caco} (>500 is great; <25 is poor), QPlogBB (-3.0 to 1.2), and PercentHumanOralAbsorption (>80% is high; <25% is poor).

In Silico Pharmacokinetic Analysis. The pharmacokinetic properties of new lead candidates are essential for the development of an effective druggable molecule. Herein, the ADME properties of Z1244904919 and Z1759961356 were calculated in QikProp (v. 4.5) (Table 3). The QikProp method is based on 1700 known oral drugs, and the rms errors of its predictions are 0.5–0.6 log unit.³¹ The ADME properties of the recently reported two SARS-CoV-2 M^{pro} inhibitors (13a and 13b)⁹ and FDA approved drug DIP,³² which have favorable pharmacokinetic properties, were also calculated and are included in Table 3. The predicted ADME values of Z1244904919 and Z1759961356 compare favorably with the drug leads 13a and 13b or FDA approved drug DIP (Table 3). Moreover, some properties, such as QPP_{Caco2} and PercentHumanOralAbsorption, are better than those of 13a, 13b, and DIP. Therefore, we are optimistic about the application of the two compounds Z1244904919 and Z1759961356 as new drug leads targeting the M^{pro} protein.

CONCLUSIONS

We report that the IC₅₀ values of the six identified inhibitors targeting M^{pro} ranged from 0.68 to 2.05 μM here. Among them, Z1244904919 and Z1759961356 inhibit the purified recombinant SARS-CoV-2 M^{pro} and their IC₅₀ values were 0.73 ± 0.04 and 0.69 ± 0.05 μM, individually. Further experiments show that Z1244904919 and Z1759961356 display inhibition against SARS-CoV-2, and EC₅₀ values were 4.98 ± and 8.52 ± μM, respectively. In addition to this, the recognized key residues that contributed to the binding modes between Z1244904919 and Z1759961356 with SARS-CoV-2 M^{pro} were elucidated by MD simulation and binding free energy analysis. The results from this study provide a new starting point for the design of antiviral drugs to treat COVID-19.

MATERIALS AND METHODS

Multiple Conformation-Based Virtual Screening.

Protein Preparation and Grid Generation. In this study, nine SARS-CoV-2 M^{pro} structures including five apo forms and four holo forms were collected from released public data. The five apo forms (no ligand bound) were extracted from 10 μs MD simulation of SARS-CoV-2 M^{pro} (PDB ID: 6LU7¹¹) per 2 μs,²⁵ and the four holo forms were homolog model (the crystal structure of SARS-CoV M^{pro} 3ATW³³ was regarded as a template) or crystal structures (PDB IDs: 6LU7,¹¹ 6Y2F,⁹ and 6Y2G⁹) of SARS-CoV-2 3CL^{pro} with diverse ligands. The Protein Preparation Wizard³⁴ was used to add hydrogen atoms, assign partial charges, assign protonation states, and minimize the structure with the OPLS3 force field³⁵ to prepare each structure. When the RMSD value reached the maximum of 0.30 Å, this minimization would be terminated. After minimization, the Receptor Grid Generation program of Glide (Version 6.8) was used to define the docking grid for each M^{pro} in the monomer state.³⁶ For each structure, by centering on the ligand (holo form) or selecting active site residues (apo form), the docking grids were generated. By using the cocrystal structure 6LU7 as a reference, the active site residues of SARS-CoV-2 3CL^{pro} in the apo form were chosen. The center and size of defined nine docking grids are summarized in Table S3.

Small Molecule Database Preparation. A protein mimetics library with 8960 commercially available compounds from Enamine was used for ensemble docking.³⁷ The library was prepared by using the LigPrep (Version 3.5) program, and

then, all compounds were processed through generating tautomers, stereoisomers, and ionization states by Epik (Version 3.2).³⁸ All the ligand preparations were under the condition of 7.0 ± 2.0 pH value with the OPLS3 force field.³⁵ QikProp (Version 4.5) was used for calculating the five compounds' ADME properties summarized in Table 3, and the library was prefiltered using druglike properties.

Ensemble Docking. Screening the prepared library via docking them into the generated grids using Glide (Version 6.8).^{36,39} High-throughput virtual screening was first carried out for maintaining 10% top-ranked structures, and those molecules were redocked on the scoring algorithm of standard precision, reserving the 10% top-scored molecules. The resulting set was further filtered at the extra precision level, and a database involving 245 compounds was retained ultimately. From the retained sub-database, 50 compounds were selected by considering the docking scores, binding mode, and scaffold diversity. Finally, 49 compounds available commercially were purchased from TargetMol for further biological evaluation.

Biacore Assay. Performing SPR experiments in a Biacore 8K device (Cytiva, Previously GE Healthcare Life Sciences) using CM5 sensor chips (Cytiva, Previously GE Healthcare Life Sciences) on the basis of the protocol provided by the manufacturer. Briefly, recombinant SARS-CoV-2 M^{pro} protein was fixed in a CM5 chip. Compounds of different concentrations were injected at a flow rate of 30 μL/min lasting for 2 min. Subsequently, collecting data for a 2 min association followed by a 5 min dissociation. The chip was regenerated by injecting 1 × PBS, 0.05% Tween-20, pH 7.4, 5% DMSO for 60 s. All procedures were run in 1 × PBS, 0.05% Tween-20, pH 7.4, 5% DMSO as a running buffer. The software Biacore Insight Evaluation Software with a 1:1 Langmuir binding model was applied to analyze the binding kinetic. The K_d was calculated by the Biacore Insight Evaluation Software.

M^{pro} Activity and Inhibition Assay. Fluorescence Resonance Energy Transfer. Chemical compounds were dissolved in 100% DMSO. Half-maximal inhibitory concentration (IC₅₀) was determined using the 3CL Protease, MBP-tagged (SARS-CoV-2) Assay Kit (BPS Bioscience, San Diego, CA, USA). In brief, 3CL protease (5 ng/μL) was preincubated with chemical compounds at indoor temperature for 30 min with slow shaking. Afterward, a substrate solution with a 50 μM final concentration was added to each well to initiate the reaction. The samples were incubated overnight at indoor temperature. The fluorescence intensity was surveyed at 360 nm excitation. GraphPad Prism 8 (GraphPad Software, San Diego, CA, USA) was used for the calculation of the IC₅₀ values.

Bioluminescence Resonance Energy Transfer. BRET was used to detect the inhibitory effect of the chemical compounds against SARS-CoV-2 M^{pro} in HEK293T cells. The 3CL protease recognition sequence linker (ITSAVLQSGFRK) was fused with enhanced yellow fluorescent protein (EYFP) and inserted into pRLuc-N2 plasmid. A full-length coding sequence of 3CL protease was inserted into pcDNA3.1-Flag plasmid. pEYFP-linker-Rluc and pcDNA3.1-3CL-Flag were co-transfected into HEK293T cells and treated with chemical compounds in different concentrations for 48 h. The BRET ratio was detected at 475 nm emission.

Antiviral Activity Assay. qRT-PCR Assay. The in vitro antiviral efficacy of compounds was determined in Vero E6

cells as previously described.¹¹ Briefly, the cells were pretreated with the chemical compound with a concentration of 10 μM for 1 h and then infected with SARS-CoV-2 with multiplicity of infection of 0.01 for 2 h. After this, the virus–drug mixture was wiped out, and the cells were placed in the medium filled with fresh drugs for further cultivation. At 72 h post infection, viral RNA (vRNA) was extracted from the culture supernatant and detected by quantitative real-time PCR (qRT-PCR).

Plaque-Reduction Assay. The anti-SARS-CoV-2 activity of selective compounds was determined through the plaque-reduction assay. Compounds in different dilution concentrations were mixed with SARS-CoV-2 (100 plaque-forming units), and 200 μL of mixtures was injected into 1×10^5 monolayer Vero E6 cells lasted for 1 h. Then, the cells were washed twice with a fresh medium; after this, the cells were incubated with 0.9% agarose containing indicated chemical compounds. After infection, at the 4th day, the cells were fixed in 4% polyoxymethylene for 30 min and finally dyed with crystal violet. The plaque-forming units were counted.

MD Simulation and Binding Free Energy Calculation.

The docking poses of Z1244904919- and Z1759961356-bound M^{Pro} complexes were used to perform MD simulation by the GPU-accelerated PMEMD module of AMBER14 software as previously described.⁴⁰ Before MD simulation, the AMBER ff14SB⁴¹ was assigned to M^{Pro} protein and Antechamber⁴² with GAFF⁴³ and RESP partial charges were applied for two inhibitors to generate the force field parameters. The HF/6-31G* level of Gaussian09 suite⁴⁴ was employed for the calculations of ligand geometric optimization and the electrostatic potential. Then, the two complexes were neutralized through adding an appropriate number of counterions and immersed into a rectangular periodic box of TIP3P⁴⁵ water molecules with an edge of 10.0 Å. For each complex, two steps of 1000 cycles of energy minimization were performed, the first one was under a harmonic restraint of a 10.0 kcal·mol⁻¹·Å⁻² force constant followed by the second minimization without restraint. After this, the two complexes were heated from 0 to 100.0 K in 2500 steps and gradually to 310.0 K within 5000 steps; both of them are under a force constant of 10.0 kcal·mol⁻¹·Å⁻². Then, equilibration with 50 ps at 310.0 K was conducted by freeing all atoms. At the end, production run with 1000 ns was performed for the two systems under the NPT ensemble at 310.0 K and 1 atm by the periodic boundary condition.

The binding free energies (ΔG_{calc}) of Z1244904919- M^{Pro} and Z1759961356- M^{Pro} complexes were calculated via the end-point molecular mechanics generalized Born surface area (MM/GBSA) approach²⁷ using the following equation (eq 1):

$$\Delta G_{\text{calc}} = \Delta E_{\text{vdW}} + \Delta E_{\text{ele}} + \Delta G_{\text{pol}} + \Delta G_{\text{nonpol}} \quad (1)$$

Furthermore, we decomposed the total binding free energy into each residue by eq 2

$$\Delta G_{\text{calc}}^{\text{per-residue}} = \Delta E_{\text{vdW}}^{\text{per-residue}} + \Delta E_{\text{ele}}^{\text{per-residue}} + \Delta G_{\text{pol}}^{\text{per-residue}} + \Delta G_{\text{nonpol}}^{\text{per-residue}} \quad (2)$$

to recognize the key residues responsible for the binding of ligand– M^{Pro} complexes.

■ ASSOCIATED CONTENT

Supporting Information

The Supporting Information is available free of charge at <https://pubs.acs.org/doi/10.1021/acs.jcim.1c00355>.

(Table S1) List of the selected 50 compounds that were predicted to bind to the active site of SARS-CoV-2 M^{Pro} ensembles; (Table S2) values of energy contribution of identified key residues in Z1244904919- M^{Pro} and Z1759961356- M^{Pro} complexes; (Table S3) summary of the origin as well as the size of the nine grid boxes used for docking; (Figure S1) result of scaffold diversity profiles of selected compounds analyzed by hierarchical clustering of the fingerprints using Tanimoto similarity and Ward's cluster linkage method; (Figure S2) binding properties of 49 computationally selected compounds at SARS-CoV-2 main protease (M^{Pro}); (Figure S3) time evolution of the root-mean-square deviation (RMSD) of backbone atoms of protein and heavy atoms of the ligand for each binding complex with respective to the initial coordinates; (Figure S4) superposition between SARS-CoV-2 M^{Pro} in complex with DIP and Z1244904919 (A) and ZN1759961356 (B), N3 and Z1244904919(C), and ZN1759961356 (D); (Figure S5) common interaction residues of Z1244904919 and Z1759961356 (filled with green color) in this study with the substrate and peptide-like inhibitor N3 (PDF)

The HPLC chromatograms and mass spectrograms of the six SARS-CoV-2 M^{Pro} inhibitors (PDF)

SARS-CoV-2 M^{Pro} conformations in the apo form (2 μs) (pdb)

SARS-CoV-2 M^{Pro} conformations in the apo form (4 μs) (pdb)

SARS-CoV-2 M^{Pro} conformations in the apo form (6 μs) (pdb)

SARS-CoV-2 M^{Pro} conformations in the apo form (8 μs) (pdb)

SARS-CoV-2 M^{Pro} conformations in the apo form (10 μs) (pdb)

SARS-CoV-2 M^{Pro} in the holo form (HM_3ATW) (pdb)

SARS-CoV-2 M^{Pro} in complex with the drug candidate M^{Pro} -Z1244904919 (pdb)

SARS-CoV-2 M^{Pro} in complex with the drug candidate M^{Pro} -Z1759961356 (pdb)

■ AUTHOR INFORMATION

Corresponding Authors

Haibo Wu – School of Life Sciences, Chongqing University, Chongqing 401331, China; Email: hbwu023@cqu.edu.cn

Weiwei Xue – School of Pharmaceutical Sciences and Innovative Drug Research Centre, Chongqing Key Laboratory of Natural Product Synthesis and Drug Research, Chongqing University, Chongqing 401331, China; orcid.org/0000-0002-3285-0574; Email: xueww@cqu.edu.cn

Authors

Jingyi Yang – School of Pharmaceutical Sciences and Innovative Drug Research Centre, Chongqing Key Laboratory of Natural Product Synthesis and Drug Research, Chongqing University, Chongqing 401331, China

Xiaoyuan Lin – School of Life Sciences, Chongqing University, Chongqing 401331, China

Na Xing – Institut für Virologie, Freie Universität Berlin, Berlin 14163, Germany

Zhao Zhang – School of Pharmaceutical Sciences and Innovative Drug Research Centre, Chongqing Key Laboratory of Natural Product Synthesis and Drug Research, Chongqing University, Chongqing 401331, China

Haiwei Zhang – Chongqing Key Laboratory of Translational Research for Cancer Metastasis and Individualized Treatment, Chongqing University Cancer Hospital, Chongqing 401331, China

Complete contact information is available at: <https://pubs.acs.org/10.1021/acs.jcim.1c00355>

Author Contributions

J.Y., X.L., and N.X. contributed equally. W.X. designed the research. J.Y., X.L., and N.X. performed the research. J.Y., X.L., N.X., Z.Z., H.Z. H.W., and W.X. analyzed the data. J.Y., H.W., and W.X. wrote the manuscript. All authors reviewed the manuscript.

Notes

The authors declare no competing financial interest.

The structure coordinates are provided in PDB files in the [Supporting Information](#). There are five SARS-CoV-2 M^{Pro} conformations in the apo form (2, 4, 6, 8, and 10 μ s.pdb) extracted from 10 μ s MD simulation,²³ one SARS-CoV-2 M^{Pro} in the holo form (HM_3ATW.pdb) modeled using the crystal structure of SARS-CoV M^{Pro} 3ATW²⁸ as a template, and the representative conformations of SARS-CoV-2 M^{Pro} in complex with two drug candidates (M^{Pro}-Z1244904919.pdb and M^{Pro}-Z1759961356.pdb). The HPLC chromatograms and mass spectrograms of the six inhibitors (Z236230776, Z1244904919, Z225729516, Z1759961356, Z108564100, and Z106460362) of SARS-CoV-2 M^{Pro} are provided in the PDF file in the [Supporting Information](#).

ACKNOWLEDGMENTS

We thank Prof. Xiaojun Yao at Lanzhou University for help and discussion on molecular docking and Prof. Zhe Li at Sun Yat-Sen University for providing the coordinates of dipyrindamole's docking pose in SARS-CoV-2 M^{Pro}. This work was funded by COVID-19 Research Grant of Chongqing Municipal Education Commission (KYYG202002), the National Natural Science Foundation of China, SGC's Rapid Response Funding for COVID-19 (No.C-0002), Technology Innovation and Application Demonstration Project of Chongqing (cstc2018jcsx-msybX0287), and Fundamental Research Funds for Central Universities (2019CDYGYB005).

ABBREVIATIONS

COVID-19, coronavirus disease 2019; SARS-CoV-2, severe acute respiratory syndrome coronavirus 2; M^{Pro} or 3CL^{Pro}, main protease; NSPs, nonstructural proteins; FRET, fluorescence resonance energy transfer; BRET, bioluminescence resonance energy transfer; DIP, dipyrindamole; SPR, surface plasmon resonance; RMSD, root-mean-square deviation; MM/GBSA, molecular mechanics generalized Born surface area; EYFP, enhanced yellow fluorescent protein; qRT-PCR, quantitative real-time PCR.

REFERENCES

(1) World Health Organization, <https://www.who.int/emergencies/diseases/novel-coronavirus-2019/technical-guidance/naming-the->

[coronavirus-disease-\(covid-2019\)-and-the-virus-that-causes-it](#) (accessed 13rd March, 2021).

(2) Wang, C.; Horby, P. W.; Hayden, F. G.; Gao, G. F. A novel coronavirus outbreak of global health concern. *Lancet* **2020**, *395*, 470–473.

(3) Wang, Y.; Li, F.; Zhang, Y.; Zhou, Y.; Tan, Y.; Chen, Y.; Zhu, F. Databases for the targeted COVID-19 therapeutics. *Br. J. Pharmacol.* **2020**, *177*, 4999–5001.

(4) Yang, J.; Zhang, Z.; Yang, F.; Zhang, H.; Wu, H.; Zhu, F.; Xue, W. Computational Design and Modeling of Nanobodies toward SARS-CoV-2 Receptor Binding Domain. *Chem. Biol. Drug Des.* **2021**, *1*.

(5) Tiwari, V.; Beer, J. C.; Sankaranarayanan, N. V.; Swanson-Mungerson, M.; Desai, U. R. Discovering small-molecule therapeutics against SARS-CoV-2. *Drug Discovery Today* **2020**, *25*, 1535–1544.

(6) Zhou, P.; Yang, X. L.; Wang, X. G.; Hu, B.; Zhang, L.; Zhang, W.; Si, H. R.; Zhu, Y.; Li, B.; Huang, C. L.; Chen, H. D.; Chen, J.; Luo, Y.; Guo, H.; Jiang, R. D.; Liu, M. Q.; Chen, Y.; Shen, X. R.; Wang, X.; Zheng, X. S.; Zhao, K.; Chen, Q. J.; Deng, F.; Liu, L. L.; Yan, B.; Zhan, F. X.; Wang, Y. Y.; Xiao, G. F.; Shi, Z. L. A pneumonia outbreak associated with a new coronavirus of probable bat origin. *Nature* **2020**, *579*, 270–273.

(7) Wu, F.; Zhao, S.; Yu, B.; Chen, Y. M.; Wang, W.; Song, Z. G.; Hu, Y.; Tao, Z. W.; Tian, J. H.; Pei, Y. Y.; Yuan, M. L.; Zhang, Y. L.; Dai, F. H.; Liu, Y.; Wang, Q. M.; Zheng, J. J.; Xu, L.; Holmes, E. C.; Zhang, Y. Z. A new coronavirus associated with human respiratory disease in China. *Nature* **2020**, *579*, 265–269.

(8) Dai, W.; Zhang, B.; Jiang, X. M.; Su, H.; Li, J.; Zhao, Y.; Xie, X.; Jin, Z.; Peng, J.; Liu, F.; Li, C.; Li, Y.; Bai, F.; Wang, H.; Cheng, X.; Cen, X.; Hu, S.; Yang, X.; Wang, J.; Liu, X.; Xiao, G.; Jiang, H.; Rao, Z.; Zhang, L. K.; Xu, Y.; Yang, H.; Liu, H. Structure-based design of antiviral drug candidates targeting the SARS-CoV-2 main protease. *Science* **2020**, *368*, 1331–1335.

(9) Zhang, L.; Lin, D.; Sun, X.; Curth, U.; Drosten, C.; Sauerhering, L.; Becker, S.; Rox, K.; Hilgenfeld, R. Crystal structure of SARS-CoV-2 main protease provides a basis for design of improved alpha-ketoamide inhibitors. *Science* **2020**, *368*, 409–412.

(10) Hilgenfeld, R. From SARS to MERS: crystallographic studies on coronavirus proteases enable antiviral drug design. *FEBS J.* **2014**, *281*, 4085–4096.

(11) Jin, Z.; Du, X.; Xu, Y.; Deng, Y.; Liu, M.; Zhao, Y.; Zhang, B.; Li, X.; Zhang, L.; Peng, C.; Duan, Y.; Yu, J.; Wang, L.; Yang, K.; Liu, F.; Jiang, R.; Yang, X.; You, T.; Liu, X.; Yang, X.; Bai, F.; Liu, H.; Liu, X.; Guddat, L. W.; Xu, W.; Xiao, G.; Qin, C.; Shi, Z.; Jiang, H.; Rao, Z.; Yang, H. Structure of M(pro) from SARS-CoV-2 and discovery of its inhibitors. *Nature* **2020**, *582*, 289–293.

(12) Gahlawat, A.; Kumar, N.; Kumar, R.; Sandhu, H.; Singh, I. P.; Singh, S.; Sjöstedt, A.; Garg, P. Structure-Based Virtual Screening to Discover Potential Lead Molecules for the SARS-CoV-2 Main Protease. *J. Chem. Inf. Model.* **2020**, *60*, 5781–5793.

(13) Ngo, S. T.; Quynh Anh Pham, N.; Thi Le, L.; Pham, D. H.; Vu, V. V. Computational Determination of Potential Inhibitors of SARS-CoV-2 Main Protease. *J. Chem. Inf. Model.* **2020**, *60*, 5771–5780.

(14) Huynh, T.; Wang, H.; Luan, B. In Silico Exploration of the Molecular Mechanism of Clinically Oriented Drugs for Possibly Inhibiting SARS-CoV-2's Main Protease. *J. Phys. Chem. Lett.* **2020**, *11*, 4413–4420.

(15) Amendola, G.; Ettari, R.; Previti, S.; di Chio, C.; Messere, A.; di Maro, S.; Hammerschmidt, S. J.; Zimmer, C.; Zimmermann, R. A.; Schirmeister, T.; Zappalà, M.; Cosconati, S. Lead Discovery of SARS-CoV-2 Main Protease Inhibitors through Covalent Docking-Based Virtual Screening. *J. Chem. Inf. Model.* **2021**, *61*, 2062–2073.

(16) Ma, C.; Sacco, M. D.; Hurst, B.; Townsend, J. A.; Hu, Y.; Szeto, T.; Zhang, X.; Tarbet, B.; Marty, M. T.; Chen, Y.; Wang, J. Boceprevir, GC-376, and calpain inhibitors II, XII inhibit SARS-CoV-2 viral replication by targeting the viral main protease. *Cell Res.* **2020**, *30*, 678–692.

(17) Jin, Z.; Zhao, Y.; Sun, Y.; Zhang, B.; Wang, H.; Wu, Y.; Zhu, Y.; Zhu, C.; Hu, T.; Du, X.; Duan, Y.; Yu, J.; Yang, X.; Yang, X.; Yang, K.;

Liu, X.; Guddat, L. W.; Xiao, G.; Zhang, L.; Yang, H.; Rao, Z. Structural basis for the inhibition of SARS-CoV-2 main protease by antineoplastic drug carmofur. *Nat. Struct. Mol. Biol.* **2020**, *27*, 529–532.

(18) Sencanski, M.; Perovic, V.; Pajovic, S. B.; Adzic, M.; Paessler, S.; Glisic, S. Drug Repurposing for Candidate SARS-CoV-2 Main Protease Inhibitors by a Novel In Silico Method. *Molecules* **2020**, *25*, 3830.

(19) Jiménez-Alberto, A.; Ribas-Aparicio, R. M.; Aparicio-Ozores, G.; Castelán-Vega, J. A. Virtual screening of approved drugs as potential SARS-CoV-2 main protease inhibitors. *Comput. Biol. Chem.* **2020**, *88*, No. 107325.

(20) Feng, Z.; Chen, M.; Xue, Y.; Liang, T.; Chen, H.; Zhou, Y.; Nolin, T. D.; Smith, R. B.; Xie, X. Q. MCCS: a novel recognition pattern-based method for fast track discovery of anti-SARS-CoV-2 drugs. *Brief. Bioinform.* **2021**, *22*, 946–962.

(21) Li, Z.; Li, X.; Huang, Y. Y.; Wu, Y.; Liu, R.; Zhou, L.; Lin, Y.; Wu, D.; Zhang, L.; Liu, H.; Xu, X.; Yu, K.; Zhang, Y.; Cui, J.; Zhan, C. G.; Wang, X.; Luo, H. B. Identify potent SARS-CoV-2 main protease inhibitors via accelerated free energy perturbation-based virtual screening of existing drugs. *Proc. Natl. Acad. Sci. U. S. A.* **2020**, *117*, 27381–27387.

(22) Bzówka, M.; Mitusińska, K.; Raczynska, A.; Samol, A.; Tuszyński, J. A.; Góra, A. Structural and Evolutionary Analysis Indicate That the SARS-CoV-2 M^{Pro} Is a Challenging Target for Small-Molecule Inhibitor Design. *Int. J. Mol. Sci.* **2020**, *21*, 3099.

(23) Suárez, D.; Díaz, N. SARS-CoV-2 Main Protease: A Molecular Dynamics Study. *J. Chem. Inf. Model.* **2020**, *60*, 5815–5831.

(24) Molecular Dynamics Simulations Related to SARS-COV-2, http://www.deshawresearch.com/resources_sarscov2.html (accessed 13rd March, 2021).

(25) Komatsu, T. S.; Okimoto, N.; Koyama, Y. M.; Hirano, Y.; Morimoto, G.; Ohno, Y.; Taiji, M. Drug binding dynamics of the dimeric SARS-CoV-2 main protease, determined by molecular dynamics simulation. *Sci. Rep.* **2020**, *10*, 16986.

(26) Sastry, M.; Lowrie, J. F.; Dixon, S. L.; Sherman, W. Large-scale systematic analysis of 2D fingerprint methods and parameters to improve virtual screening enrichments. *J. Chem. Inf. Model.* **2010**, *50*, 771–784.

(27) Wang, E.; Sun, H.; Wang, J.; Wang, Z.; Liu, H.; Zhang, J. Z. H.; Hou, T. End-Point Binding Free Energy Calculation with MM/PBSA and MM/GBSA: Strategies and Applications in Drug Design. *Chem. Rev.* **2019**, *119*, 9478–9508.

(28) Świderek, K.; Moliner, V. Revealing the molecular mechanisms of proteolysis of SARS-CoV-2 M^{Pro} by QM/MM computational methods. *Chem. Sci.* **2020**, *11*, 10626–10630.

(29) Arafet, K.; Serrano-Aparicio, N.; Lodola, A.; Mulholland, A. J.; González, F. V.; Świderek, K.; Moliner, V. Mechanism of inhibition of SARS-CoV-2 M^{Pro} by N3 peptidyl Michael acceptor explained by QM/MM simulations and design of new derivatives with tunable chemical reactivity. *Chem. Sci.* **2021**, *12*, 1433–1444.

(30) Jiang, X. R.; Yan, X.; Yu, L. P.; Liu, X. Y.; Chen, G. Q. Hyperproduction of 3-hydroxypropionate by *Halomonas bluephagenesis*. *Nat. Commun.* **2021**, *12*, 1513.

(31) Cournia, Z.; Leng, L.; Gandavadi, S.; Du, X.; Bucala, R.; Jorgensen, W. L. Discovery of human macrophage migration inhibitory factor (MIF)-CD74 antagonists via virtual screening. *J. Med. Chem.* **2009**, *52*, 416–424.

(32) Green, D.; Miller, V. The role of dipyridamole in the therapy of vascular disease. *Geriatrics* **1993**, *48*, 51–53.

(33) Akaji, K.; Konno, H.; Mitsui, H.; Teruya, K.; Shimamoto, Y.; Hattori, Y.; Ozaki, T.; Kusunoki, M.; Sanjoh, A. Structure-based design, synthesis, and evaluation of peptide-mimetic SARS 3CL protease inhibitors. *J. Med. Chem.* **2011**, *54*, 7962–7973.

(34) Madhavi Sastry, G.; Adzhigirey, M.; Day, T.; Annabhimoju, R.; Sherman, W. Protein and ligand preparation: parameters, protocols, and influence on virtual screening enrichments. *J. Comput.-Aided Mol. Des.* **2013**, *27*, 221–234.

(35) Harder, E.; Damm, W.; Maple, J.; Wu, C.; Reboul, M.; Xiang, J. Y.; Wang, L.; Lupyan, D.; Dahlgren, M. K.; Knight, J. L.; Kaus, J. W.; Cerutti, D. S.; Krilov, G.; Jorgensen, W. L.; Abel, R.; Friesner, R. A. OPLS3: A Force Field Providing Broad Coverage of Drug-like Small Molecules and Proteins. *J. Chem. Theory Comput.* **2016**, *12*, 281–296.

(36) Halgren, T. A.; Murphy, R. B.; Friesner, R. A.; Beard, H. S.; Frye, L. L.; Pollard, W. T.; Banks, J. L. Glide: a new approach for rapid, accurate docking and scoring. 2. Enrichment factors in database screening. *J. Med. Chem.* **2004**, *47*, 1750–1759.

(37) Miao, Y.; Goldfeld, D. A.; Moo, E. V.; Sexton, P. M.; Christopoulos, A.; McCammon, J. A.; Valant, C. Accelerated structure-based design of chemically diverse allosteric modulators of a muscarinic G protein-coupled receptor. *Proc. Natl. Acad. Sci. U. S. A.* **2016**, *113*, E5675–E5684.

(38) Shelley, J. C.; Cholleti, A.; Frye, L. L.; Greenwood, J. R.; Timlin, M. R.; Uchimaya, M. Epik: a software program for pK(a) prediction and protonation state generation for drug-like molecules. *J. Comput.-Aided Mol. Des.* **2007**, *21*, 681–691.

(39) Friesner, R. A.; Banks, J. L.; Murphy, R. B.; Halgren, T. A.; Klicic, J. J.; Mainz, D. T.; Repasky, M. P.; Knoll, E. H.; Shelley, M.; Perry, J. K.; Shaw, D. E.; Francis, P.; Shenkin, P. S. Glide: a new approach for rapid, accurate docking and scoring. 1. Method and assessment of docking accuracy. *J. Med. Chem.* **2004**, *47*, 1739–1749.

(40) Du, Q.; Qian, Y.; Yao, X.; Xue, W. Elucidating the tight-binding mechanism of two oral anticoagulants to factor Xa by using induced-fit docking and molecular dynamics simulation. *J. Biomol. Struct. Dyn.* **2020**, *38*, 625–633.

(41) Maier, J. A.; Martinez, C.; Kasavajhala, K.; Wickstrom, L.; Hauser, K. E.; Simmerling, C. ff14SB: Improving the Accuracy of Protein Side Chain and Backbone Parameters from ff99SB. *J. Chem. Theory Comput.* **2015**, *11*, 3696–3713.

(42) Wang, J.; Wang, W.; Kollman, P. A.; Case, D. A. Automatic atom type and bond type perception in molecular mechanical calculations. *J. Mol. Graphics Modell.* **2006**, *25*, 247–260.

(43) Wang, J.; Wolf, R. M.; Caldwell, J. W.; Kollman, P. A.; Case, D. A. Development and testing of a general amber force field. *J. Comput. Chem.* **2004**, *25*, 1157–1174.

(44) *Gaussian 09 v. D.01*. Gaussian, Inc.: Wallingford, CT, 2009.

(45) Hornak, V.; Abel, R.; Okur, A.; Strockbine, B.; Roitberg, A.; Simmerling, C. Comparison of multiple Amber force fields and development of improved protein backbone parameters. *Proteins* **2006**, *65*, 712–725.